CHALMERS
UNIVERSITY OF TECHNOLOGY

PIV Measurements Around a Generic Truck Model in Active Flow Control Experiments

13th International Symposium on Particle Image Velocimetry – ISPIV 2019
Munich, Germany, July 22-24, 2019

PIV Measurements Around a Generic Truck Model in Active Flow Control Experiments

Mikhail Tokarev[1]*, Guglielmo Minelli[2], Jie Zhang[2], Bernd R. Noack[3], Valery Chernoray[2], Siniša Krajnović[2]

[1]Kutateladze Institute of Thermophysics, SB RAS, Novosibirsk, Russia

[2]Chalmers University of Technology, M2, Fluid Dynamics, Gothenburg, Sweden

[3]LIMSI-CNRS, UPR 3251, Orsay, France

*mtokarev@itp.nsc.ru

Abstract

Trucks and buses play an important role in the global transportation figures, therefore reduction of aerodynamic drag becomes a relevant problem for road vehicles. For example, for a semi-truck moving at cruise speed, drag accounts for 60-80% of the total resistance of motion, being the largest source of power consumption. Many effective methods of drag reduction have been known from passive to active flow control. In this paper, a systematic study of a flow structure in active flow control mode around a cabin model of a semi-truck using controlled synthetic jets located at its rounded front edges (A-pillar) is carried out. Bimodal harmonic disturbances with different frequencies and amplitudes were used to control the flow. Optimization of parameters of a control signal was performed during an aerodynamic experiment in a wind tunnel by the use of an evolutionary algorithm. As a criterion of control effectiveness, weight measurements of aerodynamic drag force and energy expenditure costs for flow control were used. Further, for a set of control regimes, planar PIV measurements were performed in the flow separation zone at the side wall and in the wake behind the model. The measurements showed a decrease in the aerodynamic drag coefficient of the model by 17% compared to a baseline case without control and a significant change of the flow structure with a decrease in the thickness of the separation zone and a noticeable narrowing of the wake behind the model for some control regimes.

1 Introduction

The control of the flow around ground transport vehicles to reduce its aerodynamic drag is a relevant problem. The total global energy costs of ground transportation in 2016, according to the estimate by Davis and Boundy (2019), amounted to 84.5% of all costs, including air, sea transport, as well as pipeline transport. It is known that the drag force is proportional to the frontal area and the drag coefficient. Traditionally, one of the ways to reduce aerodynamic drag was to give objects a more aerodynamic shape to reduce the size of the separation zone and create a smoother flow around the body. Therefore, poorly streamlined vehicle bodies were equipped with various types of aerodynamic mounted elements: tractor and trailer fairings, spoilers, side skirts, flaps, etc. as reviewed in Wood and Bauer (2003). All of these examples relate to passive flow control methods, the disadvantage of which is that they are optimized for nominal flow conditions around the body.
Another method to change the flow around bodies is active flow control when the control effect on the flow can change over time due to external energy supply. The number of studies on active flow

control is less compared to the amount of research on passive control, which is technologically more mature and can be commonly found in mass production road transport.
Several papers have been published referring to experimental and numerical studies of active flow control around 3D bluff bodies. For example, in Barros et al. (2016) a fluidic actuation on the wake of a 3D blunt body is investigated. An effect of low and high frequency forcing on drag reduction at Re=2, 3 and 4×10^5 and baseline pressure recovery was analyzed. Along with the drag force and pressure measurements, particle image velocimetry (PIV) was used to assess the wake topology for different actuation strategies. Next paper by Evstafyeva et al. (2017) describes numerical simulations of flow past Ahmed body at a low Reynolds number to analyze possibilities of treating wake asymmetries by linear feedback control. Actuation was implemented by energy efficient unsteady synthetic jets acting uniformly around the perimeter of the body, just upstream of the separation. A recent work by Zhang et al. (2018) presents an experimental study of the active flow control for an Ahmed body by steady blowing. Flow diagnostics was performed at $Re = 1.7\times10^5$. PIV measurements in the wake region at streamwise and cross-flow sections at 350Hz were carried out to analyze flow structure changes during the actuation. Different combinations of actuation channels at vertical base, sides, and top of the slanted surface were tested in terms of base pressure increase and corresponding drag reduction. Maximum achieved drag reduction was 29%.
On the same line, this work is a continuation of a series of studies on the use of passive and active control methods to reduce the aerodynamic drag of 3D bluff objects such as trucks started by Chalmers University of Technology. In El-Alti et al. (2009), a series of LES calculations of the flow around a cargo trailer model was carried out with a modification of the shape of the trailer's rear part. The geometry of a boat-tailing structure with different slant angles was numerically optimized to reduce the area of the flow separation. In this case, early separation can lead to an increase of the wake area and lower base pressure. The research on drag reduction by blowing-suction in the boundary layer (BL) at the rounded A-pillars of a truck cabin model was performed by Minelli et al. (2016). Using LES numerical simulation at $Re = 10^5$, the authors observed that active control by synthetic jets in the initial region of the development of BL allows reducing aerodynamic drag by 34% for a two-dimensional model. The maximum effect is achieved when blowing-sucking perpendicular to the local flow direction. In the next paper by Minelli et al. (2017), experimental studies of active control by synthetic jets (applied at the A-pillars) were performed on a simplified truck cabin model, the same model used in this study. The evolution of the velocity fields in time near the side wall and the area behind the model by PIV with a sampling frequency of 400 Hz was reported and described. Actuation was performed using loudspeakers and single-mode forcing at selected frequencies. As a result, of the four forcing frequencies tested in the experiment, the frequencies St = 2.1 and 3.1 were detected, contributing to the early reattachment and a decrease of the thickness of the turbulent boundary layer. In Minelli et al. (2019), LES numerical simulations were compared with experiments. Experimental drag force measurements were carried out, and the advantage of the array of longitudinal slits for blowing-suction compared to one transverse slit was shown.
The purpose of this work is to measure and analyze the velocity fields obtained by 2D PIV around the model used in Minelli et al. (2017, 2019) during active flow control in the wind tunnel (WT). The optimal control laws are determined by a genetic algorithm (GA) optimizing, which determines the best frequencies and amplitudes of a bi-modal control signal while measuring the drag force.

2 Methods

Here we briefly describe the forcing system of the boundary layer (BL). The test model has a square cross section of the frontal area with a side W = 400 mm and a longitudinal extension L = 360 mm. It is designed to install interchangeable smoothed inserts to create synthetic jets in the front left and right side edges with a radius of curvature R = 20 mm. Among the inserts, one of the configurations

has 24 horizontal slots 1 mm wide and 16 mm long with a distance of 15 mm between adjacent slots. An example of the geometry of such an insert is shown in Fig. 1. As noted in Minelli et al. (2019), the array of longitudinal slits for blowing-suction is preferential compared to one transverse slit, since with this arrangement of slits the sensitivity to the spatial location of the slit on the edge of the model is significantly reduced.

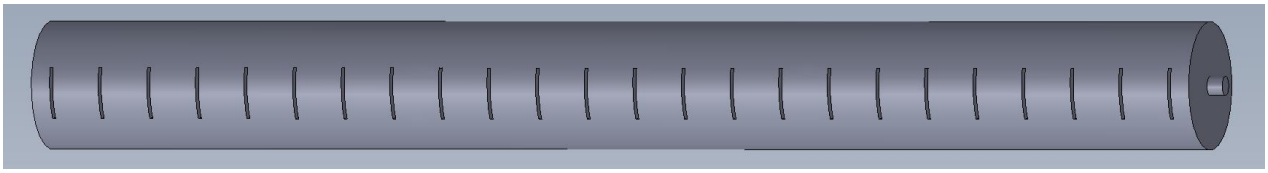

Figure 1: Example of interchangeable side insert geometry for organization of synthetic jets

Blowing and suction of the air flow through the slots was created by four Wavecor SW182BD02-01 low-frequency speakers (RMS power 62 W and 8 Ohm impedance), two for each side of the model. The speakers were connected to the ALTO MAC 2.4 stereo amplifier (max. power 900 W) to enable independent control of the actuators on the right and left sides of the model. The line inputs of the amplifier were supplied with a signal from the NI 9264 DAC via two independent channels, the output voltage of which was controlled from a LabVIEW program served as an open-loop controller because in this work the control signal did not depend on the current state of the flow.

The optimization of the forcing control signal was performed directly during the model test in WT for several hours in each case. The optimization criteria were the average value of the drag force during the evaluation of the current control signal and the energy cost for actuation. We chose 5 seconds time period for assessment of the influence of the signal on the flow. Few variants of the GA procedure, related to different types of objective function and methods of introducing forcing were tested. The first objective function (1) minimized the drag coefficient without taking other constraints into account:

$$f(Cd) = 1/Cd\ ,\ Cd = \overline{F}_d\ /(W^2 \overline{P}_{dyn})\ , \tag{1}$$

where $\overline{F}_d$ - averaged drag force, $\overline{P}_{dyn}$ - averaged dynamic pressure. The form of the second function (2) is more complex:

$$f(Cd, A) = \left\lceil \frac{1 + Cd_{base}}{1 + Cd} \right\rceil + \left\lceil \frac{k}{1 + A / A_{\max}(k-1)} \right\rceil$$

$$k = \frac{1 + Cd_{base}}{1 + Cd_{\min}};\ A = \sqrt{A_1^2 + A_2^2} \tag{2}$$

$$Cd_{base} = 0.934; Cd_{\min} = 0.7; A_{\max} = 0.2$$

It allows minimizing the drag, taking into account the energy spent for the actuation. The function is constructed in such a way that a change in *Cd* value from the baseline value to a minimum using fixed forcing amplitudes *A,* and a change in forcing amplitudes values from maximum to zero with fixed *Cd,* lead to changes in the objective function of the same order of magnitude.

The genetic algorithm was used for optimization. This algorithm of global optimization allows finding a solution that is close to optimal for a multivariable objective function in a reasonable experimental time. The genetic algorithm selects the best individuals at the end of a new generation,

creating a new population of control signals based on the cost function and the operation of crossover, elitism, and mutation, typical of a GA procedure. In this paper, the search for solutions was carried out in the four-dimensional space of features (A_1, A_2, F_1, F_2) that determine the amplitudes and frequencies of the two-mode control signal $S = A_1 \sin(2\pi F_1 t) + A_2 \sin(2\pi F_2 t)$. The next parameters of the genetic algorithm were used: population size N=60, number of generations ≥30, number of genes per variable m=25, crossover and mutation probabilities p_{cross}=0.8, p_{mut}=0.04. The optimization of the control signal parameters by the genetic algorithm was implemented in MATLAB software package and was called before each new session to estimate the current generation of signals tested in the WT.

For the flow diagnostics, we used the closed-loop WT of Chalmers University of Technology. The test section of the WT has dimensions of 3×1.8×1.25 m^3 and a velocity range is 0–60 m/s with a turbulent velocity fluctuation level of well below 0.1%. In the current experiments, the flow velocity was 20 m/s and the Reynolds number based on the characteristic size of the model W was $Re = 5\times10^5$.

The model was located symmetrically to the right and left walls of the test section, as well as in the center in the direction along the stream. The model was installed on a vertical streamlined support. The proportion of the frontal area of the model relative to the total area in the cross section of WT was 8.1%. The lower part of the support went through a hole in the floor and was fixed on a platform of a 6-component balance system. The mounting height of the model at the bottom edge was 297 mm so that the elevation of the symmetry plane of the model relative to the floor was 497 mm.

For diagnostics of an instantaneous flow topology near the model: cross-flow blowing and suction by synthetic jets, boundary layer separation on the side wall and the recirculation zone behind the model standard 2D2C PIV and Stereo PIV techniques were used (see Fig. 2). The maximum registration rate of the PIV system was 7 Hz; therefore, the obtained data were not able to track the development of the flow in time. To confront partially with the limitation of the low-speed PIV system the phase-locked sampling at the exit of the slots generating synthetic jets was performed at the place where the behavior of the flow remained coherent with the actuation signal.

The first Stereo PIV configuration is shown in Fig. 2(a). The aim of the Stereo PIV measurements was to study the effect of the single frequency actuation on the development of shear layer instabilities experimentally. The measurement plane was located at the angle $\pi/4$ to the incoming flow at a distance of 2 mm from the surface of the actuator insert, and the center of the measurement area was located at the half height of the model. Two cameras were located outside the test section one above the other. The laser sheet optics was located under the floor of the test section with a laser beam directed from bottom to top through a window. A common viewing area for the cameras included 8 slots of the insert (Fig. 1) at the middle position. At this configuration phase-locked sampling of the acquired data was used with eight different phases of the sinusoidal control signal starting from 0 with the step $\pi/8$. The frequency of the signal was 100 Hz and the amplitude 0.2 V. Typical in-plane spatial resolution for these measurements was 2 mm for a single velocity vector or two widths of the slots. Frame separation time was 16 μs.

The next 2D2C PIV configuration was used for velocity measurements in the horizontal plane of mirror symmetry at half the height of the model (see Fig. 2, b). The purpose of this configuration was to assess the effect of the optimal bi-frequency control actuation on the wake topology and turbulent boundary layer separation at the side walls. The measurement areas, camera viewing

direction, and location are shown in blue. The measurement areas were overlapped with each other for the possibility of stitching. The registration and illumination parts of the PIV system were located outside the test section, behind transparent windows as in the previous configuration. The separation time between PIV frames within a pair was 125 μs, to have particle image displacement in the range 8-9 px for undisturbed flow regions. The spatial resolution was 0.26 px/mm for the first camera and 0.31 px/mm for the second camera correspondingly.

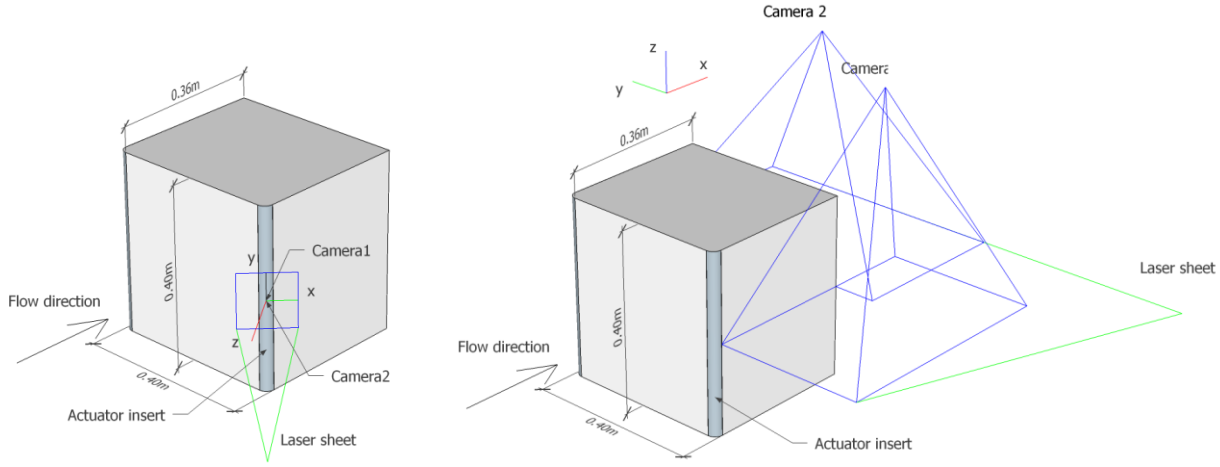

(a) Stereo PIV configuration (b) 2D2C PIV optical setup

Figure 2: PIV measurement configuration

A double-head pulsed Nd:YAG laser Quantel Evergreen 532 nm with energy 200 mJ per pulse was used in the experiments. For seeding of the flow, a fog generator SMOKE FACTORY Data II was used and a liquid based on propylene glycol solution with water. The fog was supplied downstream behind the model and accumulated in the contour of the WT. The recording of particle images started when the required concentration of tracers in the test section was reached. The image of the light scattering from particles was recorded simultaneously by two synchronized CCD ImagerProX4M cameras with a sensor size of 2048×2048 px from the LaVision FlowMaster Stereo PIV system. The cameras were equipped with either Sigma AF 105 mm f/2.8 EX DG MACRO or Nikon AF-S DX NIKKOR 35mm f/1.8G lenses with apertures f/8 and f/4 correspondingly for two setups.
For each control mode, 500 pairs of PIV images were recorded, which were processed by DaVis 8.4 software. In this study, we used the following scheme for calculating the velocity fields. The original images were preprocessed by subtracting the minimum brightness over the ensemble of images to reduce the contribution of the background signal and extract the tracer particles in the images. Next, a mask was applied to the images, removing the areas with the image of the model itself and areas with a low signal level. At the next stage, an iterative cross-correlation algorithm was used with the following parameters: 2 iterations with the initial size of the computational domain of 128×128 pixels and 50% overlap, then two more iterations with areas of 64×64 pixels and 50% overlap. To filter the velocity fields after each iteration, a median filter was used analyzing a region of 5×5 vectors.

3 Results and analysis

Results of velocity diagnostics in the region of actuation is presented in Fig. 3. It shows a typical dewarped particle image obtained at the maximum blowing stroke (2.5 ms of the 10 ms period of the single-frequency sinusoidal signal) and distribution of normal to the measurement plane mean velocity component at the same phase. Finally, mean velocity profiles for different phases in between the slots y=-7.5 mm are depicted at Fig. 3(c) for eight phases, including the case without control. As it can be seen the synthetic jets produce oscillations of the mean velocity magnitude with peak to peak difference near 8 m/s at the flow separation region with higher velocities compared to the baseline.

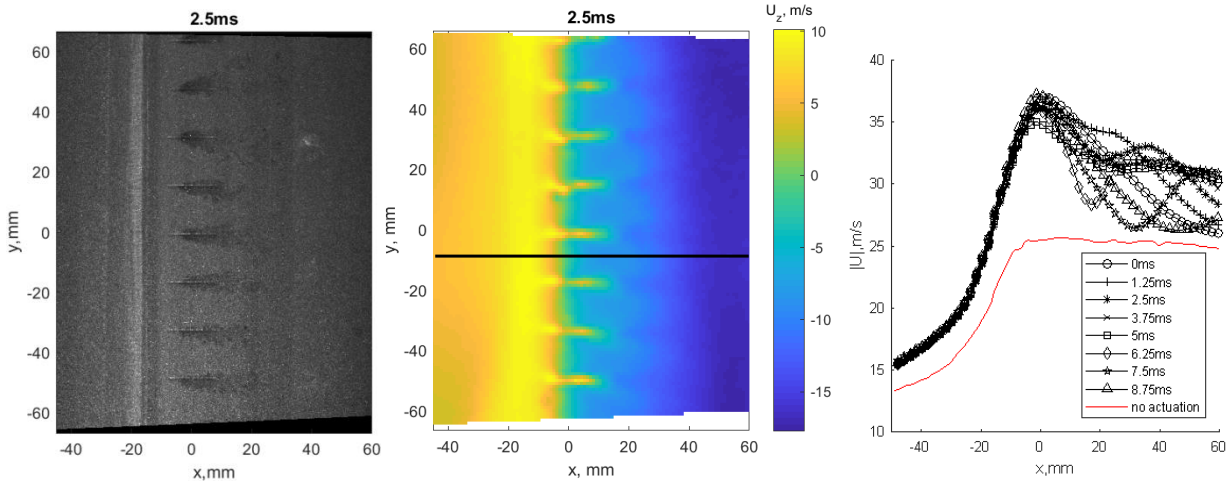

(a) Particle image at t=2.5ms (b) Ensemble average velocity field at t=2.5ms (c) Ensemble average velocity profiles at y=-7.5mm

Figure 3: Stereo PIV results with phase-locked sampling for a 100-Hz actuation signal

Control signal optimization was performed twice for determining the best bi-frequency disturbances. Two different cost functions for estimating control signals and two different ways of actuation were combined. The optimization was performed with the target function *f(Cd)* and with the function *f(Cd, A)*. In both of these cases, the disturbances were introduced in phase in the right and left sides of the model. The results of the training are shown in Fig. 4, which presents the results of the evaluation of disturbances in the initial, final, and several intermediate generations of the genetic algorithm. The disturbances are sorted by the obtained value of the fitness function in descending order, i.e., first, on the abscissa, the most promising disturbances are shown. In Fig. 5 (a) it is seen, that in the first case on the first generation a randomly selected disturbance was close enough to the optimal one, and after 30 generations it improved by 0.01 of the magnitude. The following training took into account the energy costs of the actuation, and the latest generation showed the difference between the best and worst individuals 0.1 of magnitude instead of a value of 0.17 displayed in the previous graph. Note the difference in scale of the training diagrams of Fig. 5 (a) and Fig. 5 (b).

The right column in Fig. 5 shows traces of the selected control signals for training with the functions *f(Cd)* and *f(Cd, A)*. In the first case, the best control is determined with frequencies F_1=109.5 Hz, F_2 = 221.4 Hz and amplitudes A_1 = 0.2 V, A_2 = 0.059 V. In the second case, the maximum amplitude of disturbances was ten times less with the following frequencies F_1 = 88.77 Hz, F_2 = 141.8 Hz.

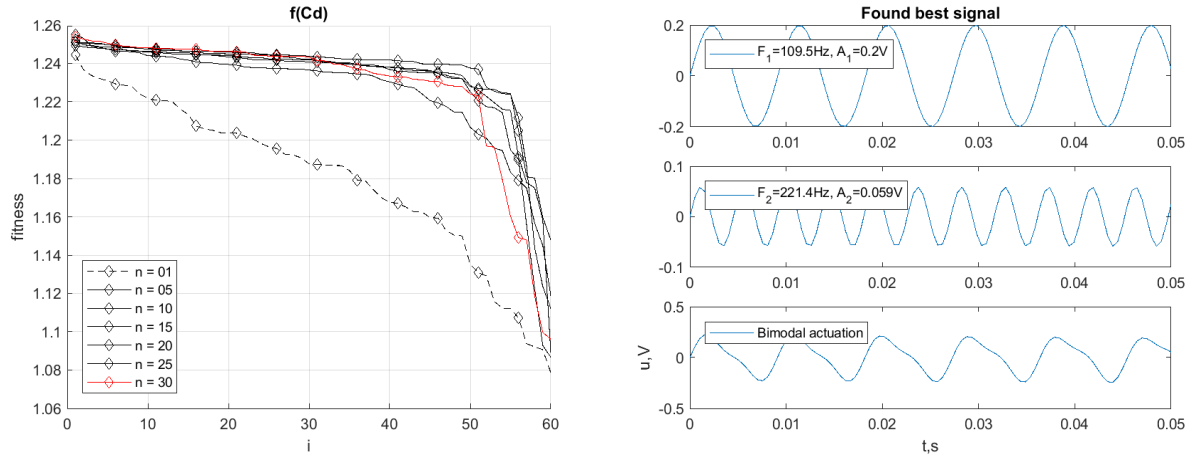

(a)

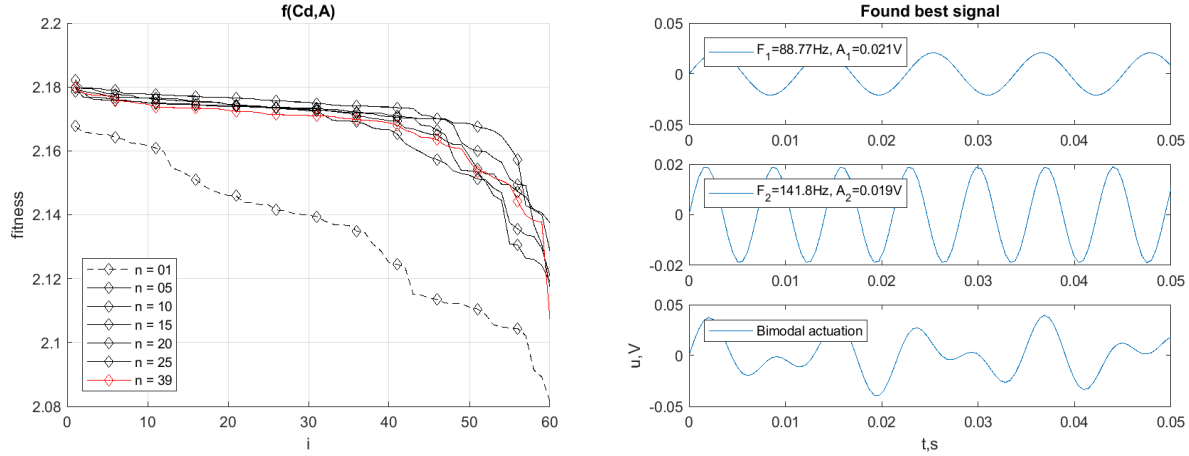

(b)

Figure 5: Dependence of the values of the objective function for individuals at different generations of training and the corresponding optimal control signal: (a) is a function *f(Cd)* with optimization of aerodynamic resistance only, (b) is a function *f(Cd, A)* with optimization of *Cd* and costs of actuation

Fig. 6 shows the distributions of the streamwise component of the average velocity near the model, obtained by the PIV method without actuation of the flow, as well as for three different control methods. Solid lines on the plots demonstrate the shape of the wake region.

Fig. 7 shows the profiles of the mean streamwise velocity in sections x = -150 and 150 mm. If we compare the two cases without actuation in Fig. 6 (a) and with control with minimal *Cd* in Fig. 6 (b), the velocity field without control is characterized by an increased boundary layer thickness (about 110 mm in the considered section), the presence of flow recirculation in the separation bubble, which is determined by negative streamwise velocity near the wall, and a wide recirculation zone in the wake behind the model. When the control is activated with a disturbance minimizing *Cd*, the turbulent boundary layer reattachment occurs, and its thickness decreases to 80 mm. The separation bubble reattachment occurs at x = -350 mm according to the data. As seen in Fig. 7 (b) in the presented section at x = 150 mm the velocity gradient across the flow increases and thus the width of the wake behind the model defined by U = 0 increases. Another feature of the wake behind the model when the disturbance is activated is the reduction of the reverse flow velocity on the

centerline axis at y = 200 mm by 2 m/s, which can be seen in Fig. 7 (b). In this case, in the reverse flow region, two local maxima of the streamwise velocity are formed instead of one maximum of the case without control. The obtained drag coefficient and the length of the wake are given in Table 1. For the case without actuation the value of the drag coefficient, *Cd* is equal to 0.958±0.004 and for the case of the best reduction the value of *Cd* is 0.794±0.003, which is 17% less.

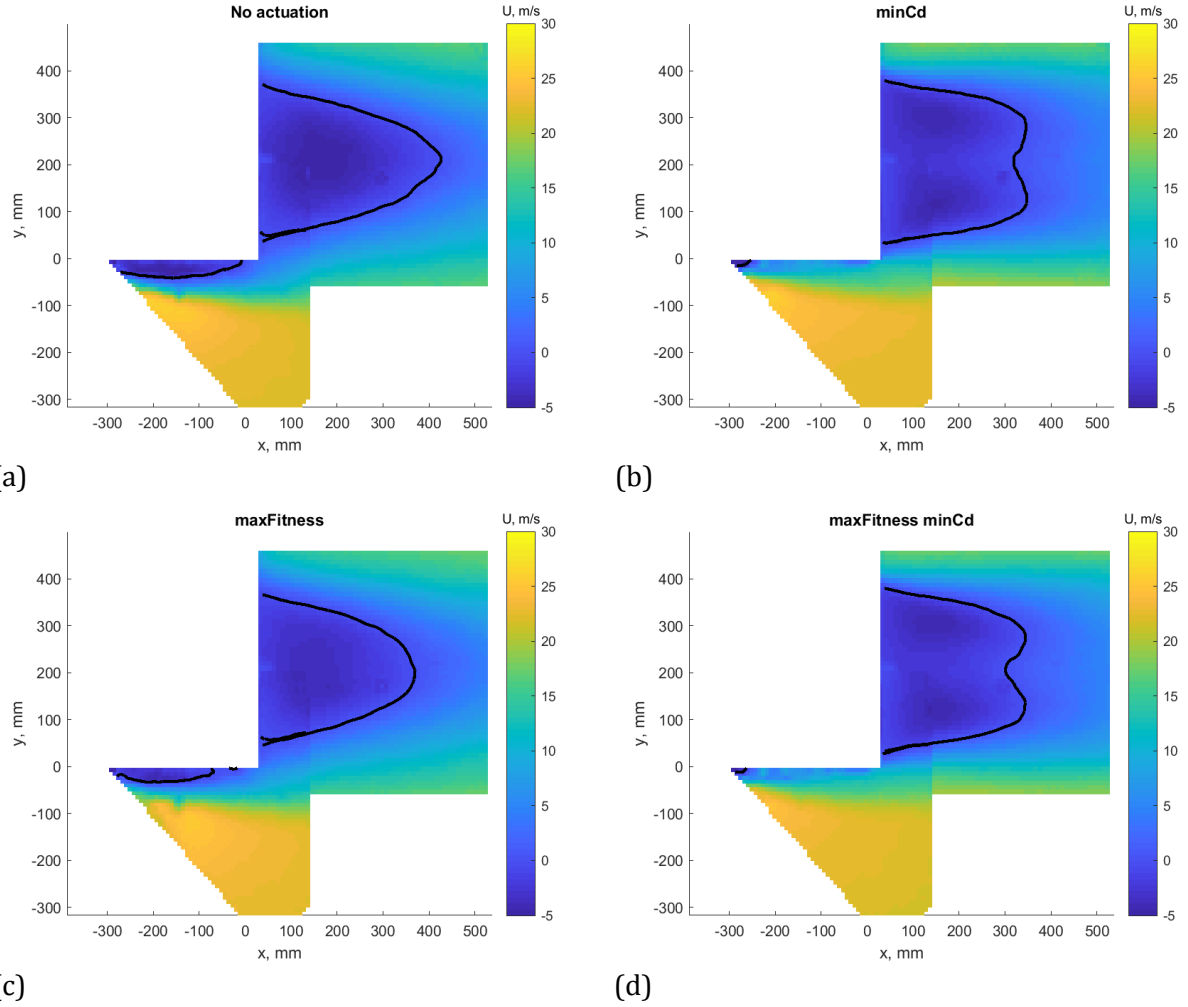

Figure 6: Spatial distributions of the mean streamwise velocity near the model for various flow control cases: (a) no control, (b) the best actuation optimized for the objective function *f(Cd)*, (c) the best actuation optimized for the objective function *f(Cd, A)*, (d) actuation which gives the minimum *Cd* taken from the last generation when training was with the objective function *f(Cd, A)*; solid lines show a contour of U=0.

It should be noted a significant advantage of the two-frequency control modes tested in this paper compared to the single-frequency actuation. With a single-frequency control, the maximum achieved drag reduction was 10% according to the results by Minelli et al. (2019) versus 17% in this work. In present work the power supplied to the actuators is 27.6 W, and power savings due to drag reduction is 88.4 W. This means that the amount of saved energy is 3.2 times higher than the energy spent for AFC. Corresponding total energy savings taking into account the costs for actuation are 8.8%.

The effect on the flow of the best actuation determined during training using the objective function *f(Cd, A)* was not so significant according to the data shown in Fig. 6 and 7,. In this case, the recirculation velocity in the separation bubble on the side wall increased from –5 m/s to –3 m/s, recirculation velocity in the wake of the model decreased by about 1 m/s and the formation of two zones with the local maximum of recirculation velocity did not occur. Measured drag coefficient for this case is 0.895±0.003, which is 6.6% lower than in the baseline case.

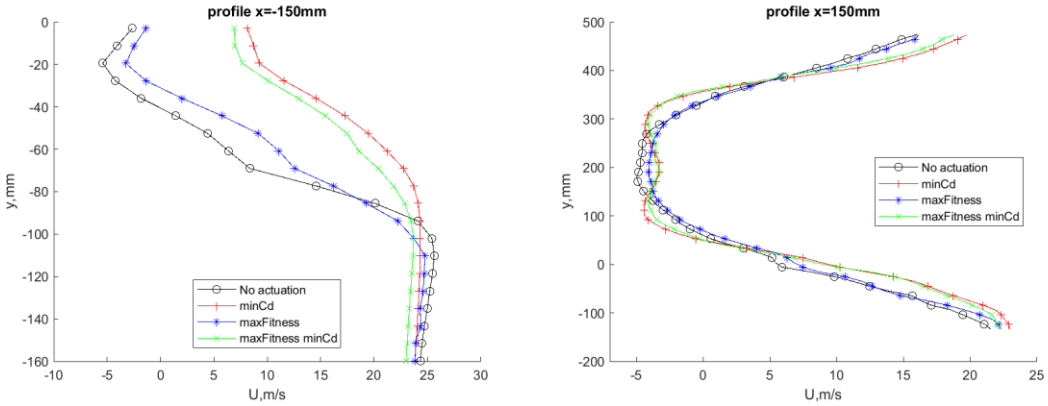

(a) (b)

Figure 7: Profiles of the mean streamwise velocity at sections: (a) x = -150 mm, (b) x = 150 mm

Table 1. Measurement data for the aerodynamic drag and wake length

Control type	$\overline{F_d}$, N	$\overline{P_{dyn}}$, Pa	*Cd*	*L/W*
No actuation	34.7±0.1	226.2±0.6	0.958±0.004	1.07
f(*Cd*)	30.28±0.1	238.0±0.6	0.794±0.003	0.85
f(*Cd,A*)	33.73±0.1	235.5±0.6	0.895±0.003	0.93
f(*Cd,A*) & minimum *Cd*	28.61±0.1	224.4±0.6	0.797±0.004	0.85

Additionally, a signal from the final generation of optimization using the function *f(Cd, A)*, leading to the minimum *Cd* was selected, and the velocity field was obtained with this control signal. The results for this case are shown in Fig. 6 (d) and Fig. 7. The value of *Cd* = 0.797±0.004 in this case and the flow structure are similar to those of the case optimizing only the drag coefficient. This means that the contribution of the reward for low amplitudes of the disturbance signal in the objective function *f(Cd, A)* outweighed the benefit of reducing the drag. Thus, when designing a target fitness function which takes into account several factors, it is necessary to carefully choose the balance of the cost of each of these components.

4 Conclusion

In this paper, systematic studies of the flow structure under active control of the flow around a generalized truck cabin model using synthetic jets located at the front rounded corners are performed. Synthetic jets are produced by oscillating membranes of the loudspeakers located inside the model. As a control signal, bi-frequency harmonic oscillations with different amplitudes and frequencies are used. The search for the optimal control parameters is carried out by a genetic algorithm, and the actuation performance is evaluated in the wind tunnel experiments at Reynolds

number Re = 5×10^5. Two objective functions are used. The first one is stimulated only by a reduction of the aerodynamic drag coefficient *Cd*, while the second one also takes into account the energy costs for actuation similar to the type of the cost function for optimal control. Diagnostics of velocity fields near the model are carried out using PIV technique.
According to the measurement results, the activation of control signals obtained using machine learning leads to a restructuring of the flow with the reattachment of the boundary layers to the side walls of the model and a decrease in the length of the wake behind the model. The drag reduction by using the control signal obtained by optimization with the first fitness function reached 17% . A significant advantage of the two-frequency control approach used in this work as compared to the single-frequency control used previously in Minelli et al. (2019) is observed (17% in this work versus 10% for the single-frequency control).

Acknowledgements

This study was funded by the Swedish Energy Agency (Energimyndigheten) with grant number 2013-003608 and supported by Volvo Trucks. The experiments were performed on resources provided by the Chalmers Laboratory of Fluids and Thermal Sciences. M. Tokarev acknowledges support in part of data processing and analysis by RSF (grant № 19-79-30075) via IT SB RAS.

References

Barros D, Borée J, Noack BR, Spohn A and Ruiz T (2016) Bluff body drag manipulation using pulsed jets and Coanda effect. *Journal of Fluid Mechanics*, 805:422

Davis SC and Boundy RG (2019) Transportation Energy Data Book, Edition 37, ORNL-5198, *Center for transportation analysis*, Oak Ridge National Laboratory, Oak Ridge, TN

El-Alti M, Kjellgren P and Davidson L (2009) Drag reduction for trucks by active flow control of the wake behind the trailer. In ICHMT DIGITAL LIBRARY ONLINE. Begel House Inc.

Evstafyeva O, Morgans AS and Dalla Longa L (2017) Simulation and feedback control of the Ahmed body flow exhibiting symmetry breaking behaviour. *Journal of Fluid Mechanics*, 817

Minelli G, Krajnović S, Basara B and Noack BR (2016). Numerical investigation of active flow control around a generic truck A-pillar. *Flow, turbulence and combustion*, 97(4):1235

Minelli G, Hartono EA, Chernoray V, Hjelm L and Krajnović S (2017). Aerodynamic flow control for a generic truck cabin using synthetic jets. *Journal of Wind Engineering and Industrial Aerodynamics*, 168:81

Minelli G, Tokarev M, Zhang J, Liu T, Chernoray V, Basara B and Krajnović S (2019) Active Aerodynamic Control of a Separated Flow Using Streamwise Synthetic Jets. *Flow Turbulence and Combustion*, In Press

Wood R and Bauer S (2003) Simple and low-cost aerodynamic drag reduction devices for tractor-trailer trucks. *SAE transactions* 112:143

Zhang BF, Liu K, Zhou Y, To S and Tu JY (2018) Active drag reduction of a high-drag Ahmed body based on steady blowing. *Journal of Fluid Mechanics*, 856:351